RESEARCH ARTICLE
doi: 10.2306/scienceasia1513-1874.2026.034

ScienceAsia 52 (2): 2026: ID 2026034: **1–8**

Preparation, characterization, and activity verification of Xylooligosaccharides from *Lablab purpureus* stalk

Wenming Jiang[a,b], **Ruixue Gong**[a], **Changyin Tang**[a], **Rujira Sukhotu**[c,*]

[a] Institute of Intelligent Manufacturing and Automobile, Chongqing Chemical Industry Vocational College, Chongqing 401228 China
[b] Chongqing Jiangbei District Disease Prevention Control Center, Chongqing 400020 China
[c] Krabi Agricultural Research and Development Center, Department of Thailand Agriculture, Krabi 81000 Thailand

*Corresponding author, e-mail: rujira22@yahoo.com

Received 25 Jul 2024, Accepted 8 Apr 2026
Available online 5 May 2026

ABSTRACT: To promote the comprehensive utilization of underutilized *Lablab purpureus* stalk, this study innovatively employs it as a raw material to produce xylooligosaccharides (XOS) and evaluates their antioxidant and prebiotic activities. Hemicellulose B was extracted via alkali treatment and deproteinized using the Sevag method, as confirmed by UV-visible spectroscopy. High-performance liquid chromatography (HPLC) analysis after hydrolysis revealed the presence of 14 monosaccharides or derivatives, predominantly xylose and arabinose. XOS were prepared through xylanase hydrolysis and characterized by scanning electron microscopy (SEM), Fourier-transform infrared spectroscopy (FT-IR), and nuclear magnetic resonance (NMR). SEM revealed a cross-linked, opaque morphology; FT-IR confirmed the presence of β-glycosidic bonds; and NMR indicated methyl/methoxy groups and 1→4 glycosidic linkages. The XOS demonstrated stronger DPPH radical scavenging capacity and reducing power than hemicellulose B and effectively promoted the growth of *Lactobacillus acidophilus* and *Bifidobacterium animalis*. This work provides a novel approach for the high-value utilization of *Lablab* stalk.

KEYWORDS: *Lablab*, crop stalk, xylooligosaccharide, prebiotic activity

INTRODUCTION

Lablab purpureus (L.) Sweet is an important tropical and subtropical legume crop cultivated in many countries worldwide, with the highest production in Asia. *Lablab* has a delicious and nutritious taste, rich in protein, fat, carbohydrates, vitamins, and more [1]. Therefore, its green beans and tender leaves are often harvested and used as vegetables. Phytochemical analysis reveals that fresh leaf extracts contain sugars, alcohols, phenols, steroids, essential oils, alkaloids, tannins, flavonoids, saponins, coumarins, terpenoids, and other substances [2, 3]. Nutritional analysis shows that *Lablab* seeds contain starch, protein, fat, trypsin inhibitors, hemagglutinin, cyanosides, oxalic acid, phytic acid, and saponins [4, 5]. *Lablab* is widely planted in Shanxi, Shaanxi, Gansu, Hebei, Henan, Hubei, Yunnan, Sichuan, and other regions of China, leading to the annual production of a significant amount of *Lablab* stalk by-products. *Lablab* stalk, as a valuable agricultural waste resource, holds significant importance in agricultural production and daily life. The common current treatment methods include using it as livestock feed [6] or incinerating it as waste. However, *Lablab* stalk contains a significant amount of hemicellulose B, which can be hydrolyzed to produce XOS.

The raw materials used to prepare XOS are primarily agricultural and forestry wastes rich in xylan. Common traditional raw materials include corncobs, bagasse, and wheat stalk [7], which are widely available and low in cost. The degradation and transformation of xylan can be achieved through enzymatic hydrolysis, chemical hydrolysis, and other processes [8]. In recent years, to diversify raw material sources and enhance the utilization of agricultural waste, leguminous crop stalk has gradually become a research focus [9]. As an agricultural by-product with extensive cultivation, *Lablab* stalk is emerging as a novel raw material for XOS production, offering economic value, ecological benefits, and easy accessibility.

XOS refer to straight-chain oligosaccharides with a degree of polymerization of 2–6. In recent years, an increasing number of researchers have started to focus on the physiological effects of functional oligosaccharides on humans and animals. XOS exhibit various physiological functions such as antibacterial properties [10], anti-inflammatory effects [11], and antioxidant activity [12]. They also demonstrate lipid-lowering effects [13] and hypoglycemic effects [14]. Consequently, they are frequently utilized as additives in pharmaceutical and food production. XOS have shown efficient selective proliferation effects on well-known intestinal probiotics like *Bifidobacterium adolescens* and *Lactobacillus plantarum* [15, 16], enhancing antibody levels and the body's ability to fight infections [17, 18]. Moreover, XOS are characterized by their safety, non-toxicity, heat resistance, and acid resistance [19]. When used with other additives, XOS do not produce adverse effects on animals. Therefore, XOS can serve as a sustainable and safe feed additive.

Due to the significant prebiotic effects of XOS, the selective conversion of agricultural and forestry

residues into XOS is currently a research hotspot. XOS, as an effective component of hemicellulose, can generally be derived from wood fiber materials rich in hemicellulose such as corn cob [20], sugarcane bagasse [21], etc. However, there is currently no research on XOS from *Lablab* stalk. To enhance the comprehensive utilization value of *Lablab*, this study prepared XOS, characterized its structure, and investigated its antioxidant and prebiotic activities.

MATERIALS AND METHODS

Extraction of hemicellulose B

Lablab purpureus (L.) Sweet stalk (provided by farmers in Changshou District of Chongqing, China) was dried and then crushed. The stalk powder was extracted by boiling in water containing 0.5% alkaline solution for 1–2 h, and then the extract was filtered with gauze. The residue from the filtration was further treated by immersing it in a boiling water bath with 0.8% ammonium oxalate for 1 h. The resulting extract was filtered again through gauze to remove impurities. The dietary fiber obtained was extracted by soaking it at 40 °C for 1–2h in a 2% sodium hydroxide solution. The extracted solution was then adjusted to pH 5 using acetic acid. Sediment was removed through filtration. To obtain a precipitate of hemicellulose B, three volumes of ethanol were added to the supernatant. The hemicellulose B was then processed using the Sevag method to eliminate proteins, followed by dialysis with a 3000 D dialysis bag to remove small molecules, and finally freeze-drying.

Protein testing

Hemicellulose B was dissolved in distilled water to reach a concentration of 1–2 mg/ml. Distilled water was used as a control, and the absorbance in the wavelength range of 200–600 nm was measured using a UV-visible spectrophotometer (UV-1800; Shanghai Precision Instrument Co., Ltd., Shanghai, China).

Monosaccharide detection

Sample of 15 mg was dissolved in 5 ml of 2 mol/l trifluoroacetic acid. Hemicellulose B was hydrolyzed at 110 °C for 2 h under nitrogen protection. After cooling, 1 ml of the hydrolysate was mixed with 1 ml of methanol. The mixture was dried with N_2 in a water bath at 70 °C. Subsequently, 1 ml of 0.3 mol/l NaOH solution was added to the dried hydrolysate to fully dissolve it.

The alkali solution of monosaccharide was mixed with 400 µl of 1-phenyl-3-methyl-5-pyrazolone methanol solution (0.5 mol/l) and allowed to react for 2 h in a water bath at 70 °C. After cooling to room temperature, the pH of the reaction solution was adjusted to 6–7 using HCl. The neutralized solution was then supplemented with 1.2 ml of water, followed by the addition of an equal volume of chloroform. After shaking, the chloroform was separated. Following two rounds of chloroform re-extraction, the aqueous solution was filtered through a 0.45 µm microporous membrane. The resulting filtrate was utilized for HPLC (LC-20A; Shimadzu Corporation, Kyoto, Japan) analysis.

Agilent 1100 (DAD detector) was used to detect monosaccharide composition. Chromatographic conditions were as follows: C18 column (250 mm × 4.6 mm); Mobile phase A: 100 mM sodium phosphate buffer (pH = 6.7); Mobile phase B: acetonitrile; Detection wavelength: 250 nm; Column temperature: 30 °C; The flow rate: 1 ml/min; The injection volume: 5 µl. Gradient elution conditions were as follows: 0 min A/B phase (86:14, v/v), 9 min A/B phase (83:17, v/v), 28 min A/B phase (78:22, v/v), 29 min A/B phase (50:50, v/v).

Enzymatic hydrolysis of hemicellulose B

Xylanase was purchased from Beijing Suolaibao Technology Co., Ltd., Beijing, China. It was produced by fermentation using *Trichoderma reesei* and has an activity of 50000 U/g. The hemicellulose B sample (0.5 g) was hydrolyzed by xylanase (200 u/g substrate) in a buffer solution with pH 4.5. The solution was hydrolyzed for 8 h at 45 °C with stirring. Samples were taken every hour and heated in a boiling water bath to inactivate the enzyme. The solution was then centrifuged at 5000 rpm for 5 min to remove the precipitate. The supernatant was hydrolyzed by sulfuric acid (6%, v:v) for 2 h. The 3,5-dinitrosalicylic acid (DNS; Shanghai McLean Biochemical Technology Co., Ltd., Shanghai, China) method was employed to determine the reducing sugar content in the supernatant and the total sugar content of the hydrolysate. The enzymolysis time was determined based on the polymerization degree. Xylose was used as the standard curve to determine the produced reducing sugar. Each sample was determined three times and the average value was taken.

Purification of XOS

Activated granular activated carbon was packed into a 22 × 400 mm chromatography column. The XOS solution was loaded into the column at a flow rate of 1 ml/min. Subsequently, the column was rinsed with 300 ml of deionized water and then eluted with a 65% ethanol solution. The ethanol was separated from the eluent using a rotary evaporator, followed by freeze-drying.

Characterization of oligosaccharides

A sample of 0.005 g of XOS was mixed with 0.5 g of KBr powder and ground together. Using KBr as the background, transmittance was measured in the wavenumber range of 4000–450 cm^{-1} using an FTIR-650 Fourier transform infrared spectrometer (Tianjin Gangdong Technology Co., Ltd., Tianjin, China).

A 5 mg sample was attached to a conductive carbon film with a double-sided adhesive. The film was then inserted into the sample chamber of ion sputtering equipment and coated with gold. Subsequently, the sample was transferred to the observation room of a scanning electron microscope (Seiss Sigma 500, Jena, Germany) and examined under an accelerated voltage of 2 kV.

The 25 mg sample was dissolved in D_2O, and the XOS spectrum was then measured at 25 °C using a 500 MHz NMR spectrometer (Bruker Corporation, Billerica, USA). Acetone was used as internal reference in the determination.

Determination of antioxidant activity *in vitro*

Sample solution of 1 ml was mixed with 4 ml of pretreated DPPH (Shanghai McLean Biochemical Technology Co., Ltd.) ethanol solution (mass fraction 0.004%) and reacted in the dark for 20–30 min at room temperature. The absorbance was measured at 517 nm. Each group of experiments was repeated three times, and the results were averaged. Significance analysis was conducted using hemicellulose B as the reference. The DPPH clearance rate is calculated as shown in Formula 1. In the formula: A_0 is the absorbance value of the DPPH ethanol solution and ethanol with the same volume; A_1 is the absorbance value of the DPPH ethanol solution and sample solution; A_2 is the absorbance value of the ethanol solution of the sample without adding DPPH.

$$E(\%) = \frac{A_0 - (A_1 - A_2)}{A_0} \times 100 \qquad \text{(Formula 1)}$$

Sample solution of 1 ml, 2.5 ml pH 6.6 mol/l phosphate buffer solution, and 2.5 ml of 1% potassium ferricyanide solution were mixed by shaking, and then bathed in water at 50 °C for 15–20 min. After cooling to room temperature, 2.5 ml of 10% trichloroacetic acid solution, 0.4 ml of 1% ferric chloride solution, and 4 ml of distilled water were added to the mixed solution. The solution was allowed to stand and react for 15–20 min. The reaction solution was centrifuged at 4000 rpm for 5 min. The absorbance of the supernatant was measured at 700 nm. Each group of experiments was repeated three times, and the results were averaged. Significance analysis was conducted using hemicellulose B as the reference. The calculation formula for reducibility is shown in Formula 2, where A_0 is the absorbance value of the blank group solution; A_1 is the absorbance value of the sample group; A_2 is the absorbance value of the control group.

$$E(\%) = \left(1 - \frac{A_1 - A_0}{A_2}\right) \times 100 \qquad \text{(Formula 2)}$$

Verification of bacterial activity

Lactobacillus acidophilus and *Bifidobacterium animalis* were activated in MRS liquid medium at 37 °C for 48 h. They were then reactivated twice using the same method. MRS liquid culture medium without glucose was prepared, and the pH was adjusted to 6.8. Two 5 ml MRS media were supplemented with 50 mg of glucose and XOS, respectively. The media were sterilized at 121 °C for 15 min and then inoculated with 5% (v/v) of the activated strains. After shaking the anaerobic culture at 37 °C, the optical density (OD) at 600 nm was measured every 4 h [19].

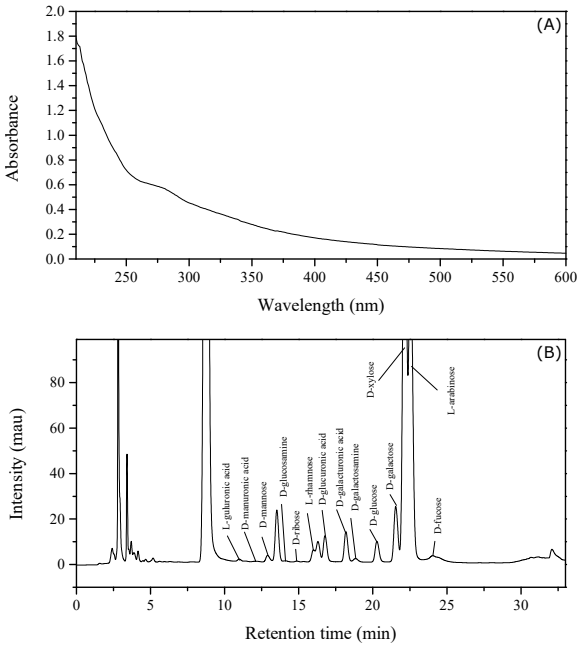

Fig. 1 Polysaccharide analysis and monosaccharide composition of plantain stem. A: UV-Vis scanning of hemicellulose B; B: Monosaccharide analysis of hemicellulose B.

Data analysis

All data are expressed as mean ± standard deviation. The experiment was repeated three times. Data were analyzed using ANOVA, with differences considered significant at $p < 0.05$ and highly significant at $p < 0.01$.

RESULTS AND DISCUSSION

Protein and monosaccharide detection

To determine if the protein in the sample has been completely removed, the absorption at 280 nm is typically assessed through ultraviolet-visible full-wavelength scanning [22]. As shown in Fig. 1A, the full-wavelength ultraviolet spectrum scanning of *Lablab* stalk hemicellulose does not exhibit a distinct absorption peak at 280 nm. This suggests that the protein in the sample has been eliminated.

HPLC is widely used in life science, food science, drug research, and environmental research. In

Table 1 Monosaccharide composition of plantain stem hemicellulose B.

No.	Monosaccharide	Retention time (min)	Mass concentration (mg/g)	Molar percentage (%)
1	L-guluronic acid	10.98	1.09	0.18
2	D-mannuronic acid	12.06	0.34	0.07
3	D-mannose	12.90	3.57	0.62
4	D-glucosamine	14.09	1.26	0.18
5	D-ribose	15.33	0.12	0.03
6	L-rhamnose	16.30	19.71	3.76
7	D-glucuronic acid	16.77	14.78	2.38
8	D-galacturonic acid	18.18	12.81	2.06
9	D-galactosamine	18.83	2.75	0.40
10	D-glucose	20.28	20.75	3.60
11	D-galactose	21.54	25.87	4.49
12	D-xylose	22.14	232.46	48.42
13	L-arabinose	22.54	152.84	31.83
14	L-fucose	24.04	10.53	2.01

polysaccharide analysis, it often uses standards as controls to analyze the composition of monosaccharides. In this study, HPLC was used to determine the composition of hemicellulose B in *Lablab* stalk. The experimental results are shown in Fig. 1B. Hemicellulose B is composed of L-guluronic acid, D-mannuronic acid, D-mannose, D-glucosamine, D-ribose, L-rhamnose, D-glucuronic acid, D-galactosamine, D-glucose, D-galactose, D-xylose, L-arabinose, and L-fucose. The contents of xylose and arabinose are relatively high, accounting for 48.42% and 31.83%, respectively (Table 1). According to the properties of monosaccharides, enzymatic hydrolysis of stalk hemicellulose B will release a lot of reducibility [23].

SEM observation of XOS

SEM is widely used to observe the morphology of nanomaterials, polymer materials, metal materials, and ceramic materials. In this study, the surface structure of XOS was observed by SEM after hemicellulose B was hydrolyzed. Fig. 2A–C show the surface structures with magnifications of 100X, 1,000X, and 10,000X, respectively. At magnification of 100X, the dried oligosaccharides are observed to cross-link into irregular fragment-like structures [24]. When magnified at 1,000X, the surface of the sample is relatively smooth with a few cracks while at magnification of 10,000X, the surface of the sample appears relatively rough.

FT-IR and one-dimensional NMR

FT-IR can determine the molecular structure and chemical information of a sample by measuring the absorption and reflection of infrared light [25]. The structure of oligosaccharides, including sugar configuration, glycosidic bond types, and functional groups, can be analyzed using FT-IR. As shown in Fig. 3A, the absorption peaks of XOS around 3500 cm^{-1} are complex, including the dynamic absorption peak of O–H, the bending vibration absorption peak of –COOH, and the absorption peak of N–H [26, 27]. The absorption peak at 1633 cm^{-1} corresponds to the stretching vibration of –OH [28]. The absorption peaks at 1414 cm^{-1} and 1378 cm^{-1} correspond to the bending deformation of $–CH_2–$ and the symmetrical deformation of $–CH_3$, respectively [29]. The absorption peak at 1331 cm^{-1} is the C–H bending vibration absorption peak [30]. The absorption peaks at 1094 cm^{-1} and 1042 cm^{-1} are the C–O absorption peaks on the sugar ring. The characteristic peak at 986 cm^{-1} indicates that sugar residues are connected by a β-glucosidic bond [31].

The NMR analysis of saccharides is used to determine the heterocephalic configuration of polysaccharides and the bonding pattern of glycosidic bonds by recording the chemical shifts of hydrogen and carbon atoms under high-frequency magnetic fields. One-dimensional NMR techniques, such as ^{1}H NMR, ^{13}C NMR, and DEPT 135, are employed to map out the chemical shifts of carbon and hydrogen atoms in sugar residues and to identify the types of carbon atoms present in oligosaccharides. In this research, the structure of XOS was elucidated using one-dimensional NMR.

The results are shown in Fig. 3B–D. It can be seen from the ^{1}H NMR spectrum (Fig. 4B) that the signal in 1 H NMR is concentrated in the range of 3.21–4.70 ppm, with a small portion distributed in the range of 1.22–1.87 ppm. Generally, the chemical shift value of α-configuration glycosyl anomeric proton is greater than 5.0 ppm, while the signal of β-glycosyl anomeric proton is less than 5.0 ppm [32]. The hydrogen spectrum signal of XOS is mainly concentrated in the range of less than 5 ppm, further confirming the glycosidic bond as β-type. The chemical shift of 3.21–4.09 ppm is mainly attributed to the hydrogen on C2–C5. The peak at 4.70 ppm corresponds to the hydrogen on C1. Additionally, the signal peaks at 1.22 ppm and 1.87 ppm are typically characteristic peaks of methyl [33].

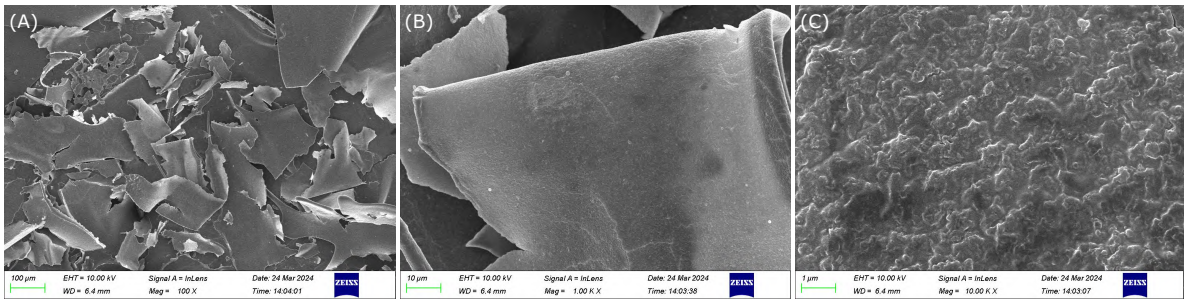

Fig. 2 SEM observation of hemicellulose B. A–C: SEM images with magnification at 100X, 1,000X and 10,000X.

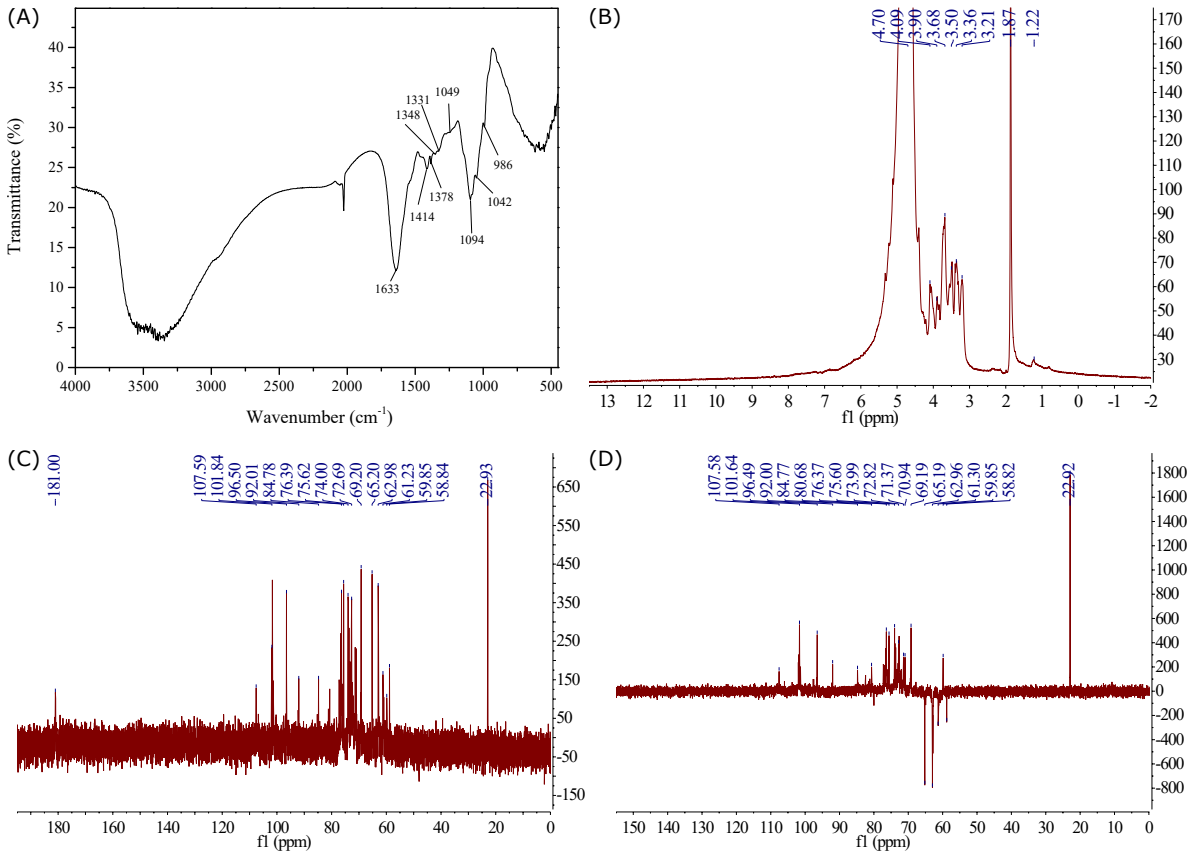

Fig. 3 FT-IR and one-dimensional NMR analysis of XOS. A: FT-IR analysis of FT-IR; B–D: ^{1}H, ^{13}C and DEPT 135 observations of XOS.

The ^{13}C NMR spectrum of XOS is shown in Fig. 4C. Peaks at 181.00 ppm chemical shift belong to the carbonyl (–CO–) signal of the aldehyde acid group. The chemical shift of C1 is 92.01–107.59 ppm. Therefore, in addition to the β-glycosidic bond, it also contains an α-glycosidic bond. The chemical shift of 62.98–84.78 ppm belongs to C2–C5. Peaks at 61.23 ppm and 58.84 ppm are attributed to C6. The signal at 22.93 ppm is the peak signal of methyl. The signal at 59.85 ppm may be attributed to methoxy [34].

In DEPT 135, CH and CH_3 exhibit positive signal peaks, while CH_2 displays negative signal peaks [35]. Based on the observations from DEPT 135 (Fig. 3C), signals are positive within the range of 92.00–107.58 ppm, which aligns with C1 in the sugar ring. The chemical shift of 69.19–84.77 ppm represents positive signal peaks, corresponding to C2–C4; 62.96–65.19 ppm indicates negative signal peaks, potentially corresponding to C5 of pentose. The negative peaks at 61.30 and 58.82 ppm are associated with C6 of certain hexoses. The signal peak at 59.85 ppm may indicate a methoxy group. Additionally, the signal peak

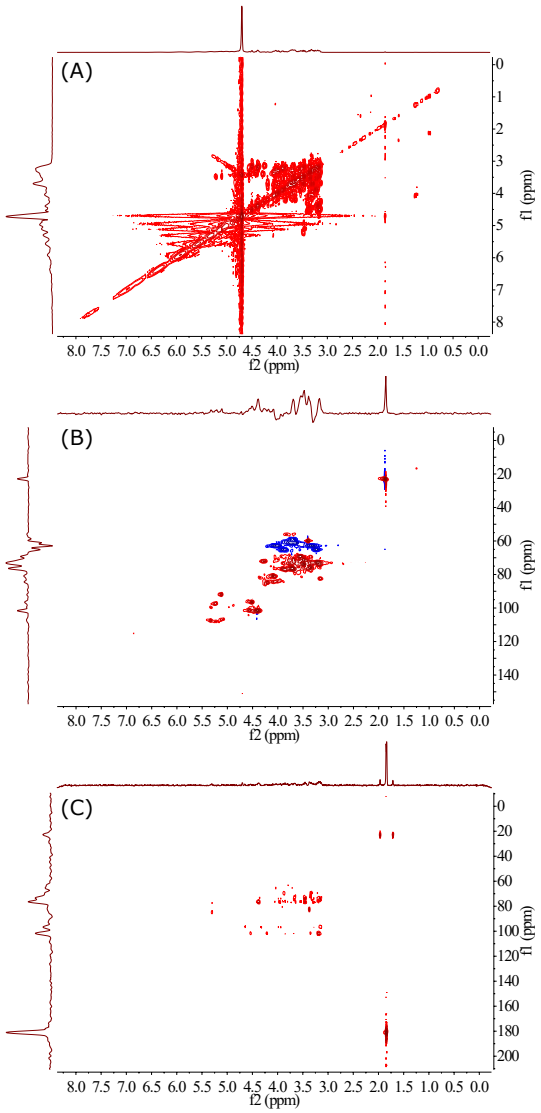

Fig. 4 Two-dimensional NMR of XOS from soybean stalk. A: COSY of XOS; B: HSQC of XOS; C: HMBC of XOS.

at 22.92 ppm corresponds to a methyl group.

Two-dimensional NMR

COSY, a commonly used homonuclear shift correlation spectrum, reveals the coupling relationships between adjacent carbons and hydrogens on the same carbon. In sugar molecules, hydrogen atoms on the same carbon intersect on the diagonal, forming diagonal peaks. As shown in Fig. 4A, the ^{1}H signal coupling of adjacent carbons is notably strong. The diagonal peak is particularly dense, indicating the coupling between methyl groups (including methoxy and acetyl groups), pentose C5, and hexose C6. Additionally, methyl and methoxy groups were identified on the diagonal.

HSQC correlates the ^{1}H nucleus with its directly connected ^{13}C nucleus and elucidates the connection relationship between C–H. Based on the analysis of the HSQC spectrum (Fig. 5B), the methyl group may be connected to C1 of the xylose residue. The hydroxyl group at C2 or C3 might be methylated to form a methoxy group. This result further confirms that XOS contains two types of groups. Methyl and methoxy groups can influence the biological activity of substances [36]. Consequently, the modifying effects of these groups have been extensively validated in studies on the functional modification of biological macromolecules, such as polysaccharides and oligosaccharides [37, 38].

HMBC spectrum is a C–H heteronuclear multibond correlation spectrum that can detect the coupling signal between hydrogen and remote carbon. From Fig. 4C, it can be observed that sugar residues are connected by 1-4 glycosidic bonds. Combined with the ^{1}H and ^{13}C spectrum, it can be inferred that the carbonyl carbon originates from the aldehyde acid structure of some sugar residues.

Activity verification

XOS produced by hemicellulose decomposition have good antioxidant and prebiotic activity. In this study, the antioxidant activity of XOS was evaluated through DPPH scavenging rate and reducibility. The prebiotic activity was assessed using *L. acidophilus* and *B. animalis* (Fig. 5). As depicted in Fig. 5A–B, the antioxidant activity and reducibility of hemicellulose B and XOS from *Lablab* stalk increased with concentration. Generally, XOS exhibited higher activity than hemicellulose B. By studying *L. acidophilus* and *B. animalis*, the growth-promoting effect of XOS from *Lablab* stalk was investigated. Fig. 5C shows that both XOS and glucose significantly promote the growth of *L. acidophilus*. Throughout the fermentation stage, XOS from *Lablab* stalk demonstrated a better growth promotion effect than glucose. The results of *Lablab* stalk XOS on the growth of *Bifidobacterium in vitro* (Fig. 5D) indicated a superior prebiotic effect of XOS. In conclusion, XOS from *Lablab* stalk can enhance the growth of *L. acidophilus* and *B. animalis* [39].

CONCLUSION

This study focused on the comprehensive utilization of *Lablab* by preparing XOS from its stalks and evaluating their antioxidant and prebiotic activities. Hemicellulose B was extracted using an alkali solution after impurity removal, and protein was eliminated via the Sevag method. UV scanning confirmed complete deproteinization. HPLC analysis showed that hemicellulose B mainly consisted of xylose and arabinose, along with other monosaccharides. XOS were then produced through xylanase hydrolysis. Structural characterizations by SEM, FT IR, and NMR revealed that XOS had a cross linked morphology, contained β glucosidic

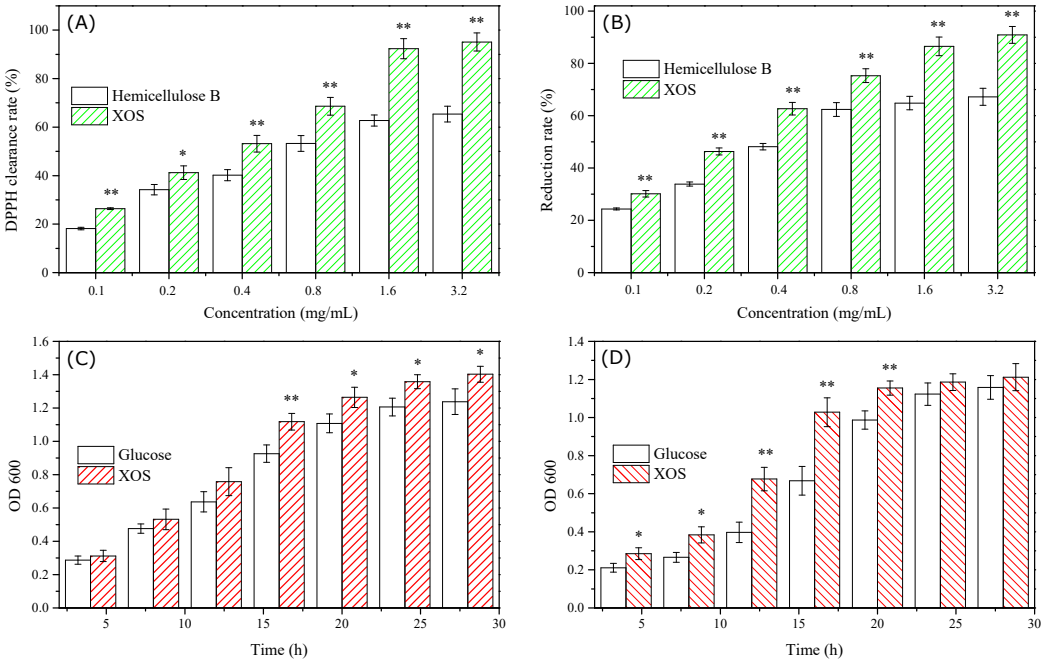

Fig. 5 Antioxidant and prebiotic activity of XOS. A: DPPH clearance of XOS; B: Reducibility of XOS; C: Prebiotic activity of XOS to *L. acidophilus*; D: Prebiotic activity of XOS to *B. animalis*.

bonds, methyl and methoxy groups, and were mainly linked by 1-4 glycosidic bonds. Antioxidant assays indicated that XOS exhibited stronger DPPH radical scavenging capacity and reducing power than hemicellulose B. Prebiotic tests demonstrated that *Lablab*-derived XOS promoted the growth of *L. acidophilus* and *B. animalis*. This research provides a basis for the high value utilization of *Lablab* stalks. However, it has limitations: the process was only performed at the laboratory scale without scale up verification, and bioactivity assessments were limited to *in vitro* experiments. Future work should focus on pilot scale studies for industrial feasibility and *in vivo* tests to further validate the biological functions and mechanisms of XOS, thus promoting its practical application.

Acknowledgements: This work was supported by Chongqing Jiangbei District 2023 Science and Health Union Medicine (Including Traditional Chinese Medicine) Research Project (Grant No. 2023-277-1-28).

REFERENCES

1. Vishnu VS, Radhamany PM (2022) Assessment of variability in *Lablab purpureus* (L.) Sweet germplasm based on quantitative morphological and biochemical traits. *Genet Resour Crop Ev* **69**, 535–1546.
2. Balekari U, Reedy CS, Krishnaveni K (2013) Antihyperglycemic and antihyperlipidaemic activities of *Dolichos lablab* seed extract on streptozotocin-nicotinamide induced diabetic rats. In: *Proc Int Conf Pharmacognosy, Phytochemistry & Natural Products* **4**, 170.
3. Deoda RS, Himarshi Pandya HP, Mital Patel MP, Yadav KN, Kadam PV, Patil MJ (2012) Antilithiatic activity of leaves, bulb and stem of *Nymphea odorata* and *Dolichos lablab* beans. *Res J Pharm, Biol Chem Sci* **3**, 814–819.
4. Al-Snafi AE (2017) The pharmacology and medical importance of *Dolichos lablab* (*Lablab purpureus*): A review. *IOSR J Pharmacy* **7**, 22–30.
5. Soetan KO (2012) Comparative evaluation of phytochemicals in the raw and aqueous crude extracts from seeds of three *Lablab purpureus* varieties. *Afri J Plant Sci* **6**, 410–415.
6. Melaku S, Peters KJ, Tegegne A (2003) *In vitro* and *in situ* evaluation of selected multipurpose trees, wheat bran and *Lablab purpureus* as potential feed supplements to tef (*Eragrostis tef*) straw. *Anim Feed Sci Tech* **108**, 159–179.
7. Valladares-Diestra KK, de Souza Vandenberghe LP, Vieira S, Goyzueta-Mamani LD, de Mattos PB, Manzoki MC, Soccol VT, Soccol CR (2023) The potential of xylooligosaccharides as prebiotics and their sustainable production from agro-industrial by-products. *Foods* **12**, 2681.
8. Akpinar O, Erdogan K, Bakir U, Yilmaz L (2010) Comparison of acid and enzymatic hydrolysis of tobacco stalk xylan for preparation of xylooligosaccharides. *LWT Food Sci Technol* **43**, 119–125.
9. Jiang W, Guo X, Liao M, Hao C, Chen J, Li F (2025) Isolation and characterization of functional oligosaccharides from soybean straw: Assessment of antioxidant and probiotic potential. *J Chem Soc Pakistan* **47**, 456.
10. Liu J, Li X, Song F, Cui S, Lu W, Zhao J, Zhang H, Gu Z, et al (2022) Dietary supplementation with low-dose xylooligosaccharide promotes the anti-Salmonella activity of probiotic *Lactiplantibacillus plantarum* ZS2058 in a murine model. *Food Res Int* **151**, 110858.
11. Sun CY, Liu Y, Feng L, Jiang WD, Wu P, Jiang J, Kuang SY, Tang L, et al (2021) Xylooligosaccharide supple-

mentation improved growth performance and prevented intestinal apoptosis in grass carp. *Aquaculture* **535**, 736360.
12. Abasubong KP, Li XF, Adjoumani JJY, Jiang GZ, Desouky HE, Liu WB (2022) Effects of dietary xylooligosaccharide prebiotic supplementation on growth, antioxidant and intestinal immune-related genes expression in common carp *Cyprinus carpio* fed a high-fat diet. *J Anim Physiol Ann N* **106**, 403–418.
13. Wang J, Cao Y, Wang C, Sun B (2011) Wheat bran xylooligosaccharides improve blood lipid metabolism and antioxidant status in rats fed a high-fat diet. *Carbohyd Polym* **86**, 1192–1197.
14. Yan F, Tian S, Du K, Xue XA, Gao P, Chen Z (2022) Preparation and nutritional properties of xylooligosaccharide from agricultural and forestry byproducts: A comprehensive review. *Front Nutr* **9**, 977548.
15. Tian S, Yang Z, Yan F, Xue XA, Lu J (2024) Preparation of xylooligosaccharides from rice husks and their structural characterization, antioxidant activity, and probiotic properties. *Int J Biol Macromol* **271**, 132575.
16. Yao D, Wu M, Wang X, Xu L, Zheng X (2022) Effect of different polymerized xylooligosaccharides on the metabolic pathway in *Bifidobacterium adolescentis*. *J Food Quality* **2022**, 4412324.
17. Hou Z, Wu D, Dai Q (2020) Effects of dietary xylo-oligosaccharide on growth performance, serum biochemical parameters, antioxidant function, and immunological function of nursery piglets. *Rev Bras Zootecn* **49**, e20190170.
18. Moure A, Gullón P, Domínguez H, Parajó JC (2006) Advances in the manufacture, purification and applications of xylo-oligosaccharides as food additives and nutraceuticals. *Process Biochem* **41**, 1913–1923.
19. Huang C, Yu Y, Li Z, Yan B, Pei W, Wu H (2022) The preparation technology and application of xylo-oligosaccharide as prebiotics in different fields: A review. *Front Nutr* **9**, 996811.
20. Yang Q, Zhang L, Lian Z, Zhang J (2023) Efficient co-production of xylo-oligosaccharides and probiotics from corncob by combined lactic acid pretreatment and two-step enzymatic hydrolysis. *Biores Techno* **382**, 129172.
21. Zhai Y, Yao S, Zhang L, Huang R, Xu Y, Zhou X, Jiang K (2024) Xylooligosaccharides and glucose preparation from sugarcane bagasse by a combination of acetic acid treatment and sequential xylanase and cellulase enzymatic hydrolysis. *Ind Crop Prod* **210**, 118202.
22. Arvind P, Priyadarshini S, Duraiswamy B, Dhanabal SP, Ramu G (2021) UV detection and avoidance of protein in *Basella alba* leaf mucilage polysaccharide by differential precipitation. *Res J Pharmacy Technol* **14**, 3093–3096.
23. Valls C, Pastor FJ, Vidal T, Roncero MB, Díaz P, Martínez J, Valenzuela SV (2018) Antioxidant activity of xylooligosaccharides produced from glucuronoxylan by Xyn10A and Xyn30D xylanases and eucalyptus autohydrolysates. *Carbohyd Polym* **194**, 43–50.
24. Penksza P, Juhász R, Szabó-Nótin B, Sipos L (2020) Xylo-oligosaccharides as texture modifier compounds in aqueous media and in combination with food thickeners. *Food Sci Nutr* **8**, 3023–3030.
25. Sorawit NN, Wichanee B, Hunsa P, Sehanat P, Pongtharin L (2026) Enzymatic hydrolyses of glucurono(arabino)xylan from two pasture crops, purple guinea (*Panicum maximum* TD58) and Napier (*Pennisetum purpureum* × *Pennisetum americanum*) grasses. *ScienceAsia* **52**, ID 2026015.
26. Carson L, Kelly-Brown C, Stewart M, Oki A, Regisford G, Luo Z, Bakhmutov VI (2009) Synthesis and characterization of chitosan-carbon nanotube composites. *Mater Lett* **63**, 617–620.
27. Nejatzadeh-Barandozi F, Enferadi ST (2012) FT-IR study of the polysaccharides isolated from the skin juice, gel juice, and flower of Aloe vera tissues affected by fertilizer treatment. *Bioorg Med Chem Lett* **2**, 1–9.
28. Thombare N, Mahto A, Singh D, Chowdhury AR, Ansari MF (2023) Comparative FTIR characterization of various natural gums: A criterion for their identification. *J Polym Environ* **31**, 3372–3380.
29. Zeng Q, Wang Y, Javeed A, Chen F, Li J, Guan Y, Chen B, Han B (2024) Preparation and properties of polyvinyl alcohol/chitosan-based hydrogel with dual pH/NH_3 sensor for naked-eye monitoring of seafood freshness. *Int J Biol Macromol* **263**, 130440.
30. Rajora AD, Bal T (2023) Evaluation of cashew gum-polyvinyl alcohol (CG-PVA) electrospun nanofiber mat for scarless wound healing in a murine model. *Int J Biol Macromol* **240**, 124417.
31. Hong T, Yin JY, Nie SP, Xie MY (2021) Applications of infrared spectroscopy in polysaccharide structural analysis: Progress, challenge and perspective. *Food Chem X* **12**, 100168.
32. Huang SQ, Li JW, Li YQ, Wang Z (2011) Purification and structural characterization of a new water-soluble neutral polysaccharide GLP-F1-1 from *Ganoderma lucidum*. *Int J Biol Macromol* **48**, 165–169.
33. Cheng HN, Neiss TG (2012) Solution NMR spectroscopy of food polysaccharides. *Polym Rev* **52**, 81–114.
34. Fischer T, Yair A, Veste M, Geppert H (2013) Hydraulic properties of biological soil crusts on sand dunes studied by ^{13}C-CP/MAS-NMR: A comparison between an arid and a temperate site. *Catena* **110**, 155–160.
35. Cordeiro LM, de Fátima Reinhardt V, Baggio CH, de Paula Werner MF, Burci LM, Sassaki GL, Iacomini M (2012) Arabinan and arabinan-rich pectic polysaccharides from quinoa (*Chenopodium quinoa*) seeds: Structure and gastroprotective activity. *Food Chem* **130**, 937–944.
36. Li C, Dai T, Chen J, Chen M, Liang R, Liu C, Du L, McClements DJ (2023) Modification of flavonoids: Methods and influences on biological activities. *Crit Rev Food Sci* **63**, 10637–58.
37. Zhao T, Yang M, Ma L, Liu X, Ding Q, Chai G, Lu Y, Wei H, et al (2023) Structural modification and biological activity of polysaccharides. *Molecules* **28**, 5416.
38. Ge X, Zhu S, Yang H, Wang X, Li J, Liu S, Xing R, Li P, et al (2024) Impact of O-acetylation on chitin oligosaccharides modulating inflammatory responses in LPS-induced RAW264.7 cells and mice. *Carbohyd Res* **542**, 109177.
39. Mäkeläinen H, Saarinen M, Stowell J, Rautonen N, Ouwehand AC (2010) Xylo-oligosaccharides and lactitol promote the growth of *Bifidobacterium lactis* and *Lactobacillus* species in pure cultures. *Benef Microbes* **1**, 139–148.